AIAA Guidance, Navigation, and Control Conference
2 - 5 August 2010, Toronto, Ontario Canada

AIAA 2010-7857

Full Envelope Modular Adaptive Control of a Fighter Aircraft using Orthogonal Least Squares

E.R. van Oort*, L. Sonneveldt†, Q.P. Chu‡, J.A. Mulder§

Delft University of Technology, P.O. Box 5058, 2600 GB Delft, The Netherlands

Downloaded by TECHNISCHE UNIVERSITEIT DELFT on December 30, 2013 | http://arc.aiaa.org | DOI: 10.2514/6.2010-7857

A new adaptive nonlinear flight controller is designed for a high fidelity, six degrees of freedom F-16 model for the entire flight envelope. The design is based on a modular approach which separates the design of the control law and the online identifier. The control law design is based on backstepping with nonlinear damping terms to robustify the design against parameter estimation errors and unknown bounded disturbances. The flight envelope is partitioned into hyperboxes, for each hyperbox a locally valid incremental model is estimated based on the linearized equations of motion. A continuous-time formulation of orthogonal least squares is used for identification of these locally valid models. The obtained local models are interpolated by means of B-splines to obtain a smooth model valid for the complete flight envelope. The performance of the resulting nonlinear adaptive control design is evaluated on the F-16 aircraft model for representative flight conditions, maneuvers, and failure cases.

Nomenclature

α, β	Angle of attack, sideslip angle	rad
$\bar{c}$	Reference chord length	m
$\bar{q}$	Dynamic pressure	N/m^2
$\bar{X}, \bar{Y}, \bar{Z}$	Total aerodynamic forces in the body coordinate system	N
$\delta_a, \delta_e, \delta_r$	Control surface deflections	rad
ϵ	Estimation error	
Γ	Adaptive bounding gain matrix > 0	
κ	Nonlinear damping gain matrix > 0	
$\langle x, y \rangle$	$\int_0^t \exp^{\lambda(\tau - t)} x(\tau) y(\tau)^T d\tau$	
$\mathbf{J}$	Inertia tensor	kgm^2
ω_B	Angular velocity in the body coordinate system	rad/s
$\otimes$	Kronecker product	
σ	Leakage gain > 0	
ϑ	Unknown parameter	
b	Reference span	m
C_i	Tracking error gain matrix > 0	
L_0, M_0, N_0	Aerodynamic trim moments in body coordinate system	Nm
$L_{\delta_\star}, M_{\delta_\star}, N_{\delta_\star}$	Aerodynamic moment derivative with respect to control surface $\star$	Nm
p_S, q_S, r_S	Stability-axes rotational rates	rad/s
p_{static}	Static pressure	N/m^2
S	Total wingarea	m^2
$T_{B \to S}$	Transformation matrix from body to stability coordinate system	
V_T	Total airspeed	m/s

*PhD Student, ASTI, e.r.vanoort@tudelft.nl, AIAA Student Member.
†PhD Student, ASTI, AIAA Student Member.
‡Associate Professor, Control and Simulation Division, Faculty of Aerospace Engineering, AIAA Member.
§Professor, Control and Simulation Division, Faculty of Aerospace Engineering, AIAA Member.

Copyright © 2010 by Delft University of Technology. Published by the American Institute of Aeronautics and Astronautics, Inc., with permission.

Downloaded by TECHNISCHE UNIVERSITEIT DELFT on December 30, 2013 | http://arc.aiaa.org | DOI: 10.2514/6.2010-7857

I. Introduction

During the last decades the flight envelope of modern fighter aircraft has become larger, and in this expanded flight envelope the performance requirements have become more demanding. Examples of modern aircraft with large flight envelopes are the F-22 Raptor and F-35 Lightning II. Most modern fighters are capable of flying at high angles of attack, and high angles of sideslip to achieve high maneuverability. At these flight conditions, unmodeled vehicle dynamics and unmodeled parametric variations can occur, due to unsteady aerodynamic effects, control surface saturation and increased longitudinal and lateral coupling.[1] In addition to this, there is an increased interest in the ability of aircraft to remain controllable and operable after faults, failures and structural damage occurring during the flight. Because of these challenges, advanced nonlinear adaptive control techniques are typically required to address the nonlinear, uncertain and time-varying, characteristics and requirements of such vehicles.

Among the popular advanced control design methods for these uncertain and nonlinear systems are model-based control techniques such as Nonlinear Dynamic Inversion (NDI),[2,3] adaptive backstepping,[4,5] Model Reference Adaptive Control (MRAC)[6,7] and variable structure control (VSC).[8,9] The main advantages of these methods are that they avoid the time consuming and costly gain-scheduling process, offer larger flexibility for handling evolving models during progessive model development stages, and possess greater ability to address nonstandard flight regimes. Some examples of such methods applied to full envelope flight control are Ref. 10 using NDI with Recursive Least Squares (RLS) estimation of aerodynamic derivatives of a linearized single flight condition model, NDI combinations with Neural Networks (NN) are designed and applied in Refs. 1, 11–13. Refs. 14, 15 use integrated adaptive backstepping with B-spline networks to approximate the aerodynamic derivatives, backstepping in combination with NN aproximation is applied in Refs. 16–18. A hybrid combination of NDI and MRAC NN control is used in Ref. 19, and Refs. 20, 21 apply direct adaptive control with NN. Variable structural control is applied in Refs. 22, 23 yet limited to single flight condition models.

In this paper a modular approach based on backstepping is taken, extending earlier work 10, 24 to full flight envelope model identification, and applying it on a high fidelity nonlinear model. Until now this approach has only been used on single flight condition models with non-varying parameters. The control law is based on Input-to-State Stable (ISS) backstepping which can be combined with any identifier that guarantees bounded estimates. Command filters are used to avoid the tedious analytic computation of virtual control signal derivatives, and make it possible to apply the control design to non-lower triangular systems. The flight envelope is partitioned into hyperboxes, in each of these boxes an incremental locally valid linear-in-the-parameters model is estimated using continuous-time orthogonal least squares. The benefit of this partitioning approach over a single local model approach is that information can be stored, such that when revisiting a identified part of the flight envelope the estimated incremental model can be retrieved instead of re-identified. The output of the hyperboxes is combined using tensor-product B-spline weights to obtain a smooth, nonlinear and globally valid dynamic aircraft model. Compared to multilayer neural network approaches the advantages of the B-splines are their local support and numerical stability. This local support allows updating the estimated model only at the current flight condition. Additionally, it is easier to extract model information for health monitoring and failure analysis from a model with clear physical interpretation.[25]

The paper is organized as follows. Section II introduces the modular control design using backstepping. Section III discusses the identification design, the orthogonal least squares identification method and the flight envelope partitioning. In Section IV the method is applied to a model of the F-16 aircraft. Section V introduces the simulation experiment, and a discussion of the results. Section VI presents the conclusions.

II. Adaptive Controller Design

Consider a nonlinear system

$$\begin{aligned} \dot{\mathbf{x}} &= \mathbf{g}(\mathbf{x},\mathbf{u}) \\ \mathbf{y} &= \mathbf{h}(\mathbf{x}) \end{aligned} \tag{1}$$

where $\mathbf{x} \in \mathbb{R}^n$ is the state vector, $\mathbf{u} \in \mathcal{U} \subset \mathbb{R}^m$ is the system control vector, and $\mathbf{y} \in \mathbb{R}^p$ is the output vector. The function $\mathbf{g}$ contains both parametric and nonparametric uncertainties. The control objective is to let the system output track a known smooth reference signal $\mathbf{y}_r$ with bounded derivatives. In the modular backstepping approach the design of the identifier and control law is separated. This allows for

more flexibility in the choice of identification method, which is therefore not limited to Lyapunov-based identifier designs. Thus, the identification process is not only driven by the tracking error, the system state and/or its measurements can be incorporated as well by means of nonlinear swapping filters. For linear systems the separation principle[26] holds, which allows straightforward separation of the identifier and control law. The true parameter values are simply replaced by their estimates in the control law according to the certainty equivalence principle.[4,27] However, due to the difference in stability characteristics of linear and nonlinear systems this is not allowed for general nonlinear systems. In systems with faster than linear growing nonlinearities (for example x^2 and $x_1 x_2$) even a small parameter estimation error can drive the state to infinity in finite time.[4] Hence, the control law has to be made robust against estimation errors and the time varying character of the parameter estimates. The estimation error is viewed as unknown disturbance and is attenuated by adding nonlinear damping terms to the control law. The complete structure of the proposed control design is shown in Fig. 1.

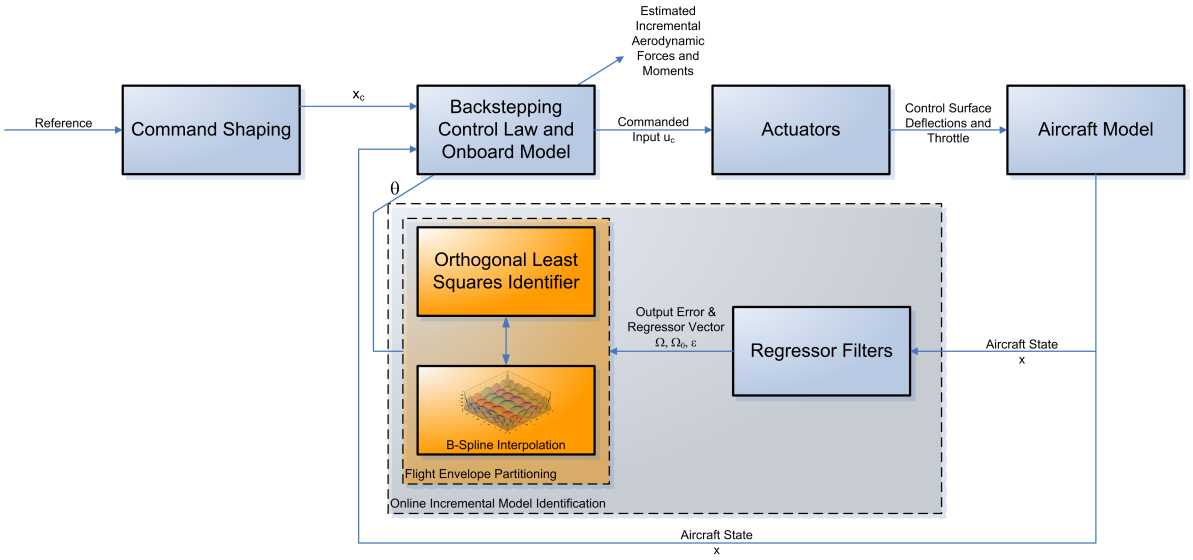

Figure 1. A schematic overview of the control architecture.

II.A. System dynamics

First of all rewrite the system dynamics (1) to

$$\begin{aligned} \dot{\mathbf{x}}_i &= \mathbf{f}_i(\mathbf{x},\mathbf{u}) + \mathbf{B}_i(\mathbf{x})\mathbf{x}_{i+1} + \varphi_i^T(\mathbf{x},\mathbf{u})\vartheta + \delta_i(\mathbf{x},\mathbf{u},t) \\ \dot{\mathbf{x}}_n &= \mathbf{f}_n(\mathbf{x}) + \left(\mathbf{B}_{n_0}(\mathbf{x}) + \mathbf{B}_{n_\vartheta}(\mathbf{x},\vartheta)\right)\mathbf{u} + \varphi_n^T(\mathbf{x},\mathbf{u})\vartheta + \delta_n(\mathbf{x},\mathbf{u},t) \end{aligned} \tag{2}$$

where δ represents unknown bounded disturbances, $\mathbf{f}_i$, $\mathbf{B}_i$ and $\mathbf{B}_{n_0}$ represent known parts of the system dynamics, $\mathbf{B}_{n_\vartheta}$ uncertainty in the control effectiveness, $\varphi^T : \mathbb{R}^n \times \mathbb{R}^m \to \mathbb{R}^{n\times p}$ a known matrix function , and $\vartheta \in \mathbb{R}^q$ an unknown constant vector of parameters, together these present the uncertain, or unknown part of the dynamics to be estimated. Assume that the disturbances δ are bounded as

$$|\delta(\mathbf{x},\mathbf{u},t)| \leq \mathbf{p}^T(\mathbf{x},\mathbf{u})\psi^\star \;\; \forall \mathbf{x} \in \mathbb{R}^n, \;\; \forall \mathbf{u} \in \mathbb{R}^m, \;\; \forall t \in \mathbb{R}^+ \tag{3}$$

where $\mathbf{p} \geq 0$ is a vector of known smooth functions, and $\psi^\star \geq 0$ is an unknown constant parameter vector defining an upper bound on the uncertainty.

II.B. Backstepping Control Law Design

The ISS-backstepping scheme from Ref. 4,5 is combined with the command filtering approach and adaptive bounding techniques from Refs. 15, 28, 29. Using this combination, the tedious analytical computation of derivatives of the intermediate control laws is avoided, the backstepping method can be applied to systems which are not in lower triangular form, and magnitude and rate constraints on the (virtual) control law can

Downloaded by TECHNISCHE UNIVERSITEIT DELFT on December 30, 2013 | http://arc.aiaa.org | DOI: 10.2514/6.2010-7857

be incorporated. The adaptive bounding has been included to robustify the design against the mismatch between the output of the interpolated linear local models and the true system. The control law design can be summarized as

$$
\begin{aligned}
\mathbf{z}_i &= \mathbf{x}_i - \mathbf{x}_{i_c} - \xi_i, && \text{(4a)}\\
\dot{\mathbf{e}}_i &= \mathbf{z}_i, && \text{(4b)}\\
\dot{\xi}_i &= -C_i\xi_i + \mathbf{B}_i\left(\mathbf{x}_{i+1_c} - \mathbf{x}^0_{i+1_c}\right), && \text{(4c)}\\
\mathbf{x}^0_{i_c} &= \alpha_{i-1} - \xi_i, && \text{(4d)}\\
\omega_i &= p_i(\mathbf{x})\tanh\left(\frac{\mathbf{x}_i - \mathbf{x}_{i_c}}{\varsigma_i}\right), && \text{(4e)}\\
\beta_i &= \psi_i\omega_i, && \text{(4f)}\\
\dot{\psi}_i &= \Gamma_i\left(\omega_i\mathbf{z}_i - \sigma_i(\psi_i - \psi_0)\right), && \text{(4g)}\\
\alpha_i &= \mathbf{B}_i^{-1}\left(-\mathbf{f}_i - \varphi_i^T\hat{\vartheta} - C_1\left(\mathbf{x}_i - \mathbf{x}_{i_c}\right) - S_i\mathbf{z}_i + \dot{\mathbf{x}}_{i_c} - K_i\mathbf{e}_i - \beta_i - \mathbf{B}_{i-1}^T\mathbf{z}_{i-1}\right), && \text{(4h)}\\
S_i &= \varphi_i^T\kappa_i\varphi_i, && \text{(4i)}\\
\mathbf{u}^0_c &= \hat{\mathbf{B}}_n^{-1}\mathbf{B}_n\alpha_n - \hat{\mathbf{B}}_n^{-1}\kappa_u\mathbf{z}_n, && \text{(4j)}
\end{aligned}
$$

where $\mathbf{z}$ is the augmented tracking error, ξ a filtered version of the error $(x_{i+1_c} - x^0_{i+1_c})$ imposed by the command filter, $\mathbf{e}$ is the integrated augmented tracking error, $\mathbf{x}^0_c$ the filter input, α_i the virtual control input at stage i. $\hat{\mathbf{B}}_\mathbf{n}$ is the estimate of $\mathbf{B}_n = \mathbf{B}_{n_0} + \mathbf{B}_{n_\vartheta}$, $\sigma_i \geq 0$ is a constant leakage gain to guarantee boundedness of ψ_i, $\psi_i^0 \geq 0$ is a design constant Nonlinear damping, through S_i, is used to guarantee boundedness of the states with respect to the parameter estimation error. The parameter ς_i is a (small) constant used to smooth the switching at $\omega_i = 0$.

Application of the design (4) to the system (2) results in the augmented tracking error derivatives for $i = 1, \ldots, n-1$, the compensated tracking error dynamics become

$$
\begin{aligned}
\dot{\mathbf{z}}_i &= \mathbf{f}_i + \mathbf{B}_i\mathbf{x}_{i+1} + \varphi_i^T\vartheta + \delta_i - \dot{\mathbf{x}}_{i_c} - \dot{\xi}_i\\
&= \mathbf{f}_i + \mathbf{B}_i\mathbf{x}^0_{i+1_c} + \mathbf{B}_i(\mathbf{x}_{i+1_c} - \mathbf{x}^0_{i+1_c}) + \mathbf{B}_i(\mathbf{x}_{i+1} - \mathbf{x}_{i+1_c}) + \varphi_i^T\vartheta + \delta_i - \dot{\mathbf{x}}_{i_c} + C_i\xi_i\\
&\quad -\mathbf{B}_i(\mathbf{x}_{i+1_c} - \mathbf{x}^0_{i+1_c})\\
&= \mathbf{f}_i + \mathbf{B}_i\alpha_i + \mathbf{B}_i(\mathbf{x}_{i+1} - \mathbf{x}_{i+1_c} - \xi_{i+1}) + \varphi_i^T\vartheta + \delta_i - \dot{\mathbf{x}}_{i_c} + C_i\xi_i\\
&= -(C_i + S_i)(\mathbf{x}_i - \mathbf{x}_{i+1_c} - \xi_i) + \mathbf{B}_i(\mathbf{x}_{i+1} - \mathbf{x}_{i+1_c} - \xi_{i+1}) + \varphi_i^T\tilde{\vartheta} + \delta_i - \beta_i - K_i\mathbf{e}_i - \mathbf{B}_{i-1}^T\mathbf{z}_{i-1},
\end{aligned}
\tag{5}
$$

with $B_0 = z_0 = 0$. For $\mathbf{z}_n$ they become

$$
\begin{aligned}
\dot{\mathbf{z}}_n &= \mathbf{f}_n + \mathbf{B}_n\mathbf{u} + \varphi_n^T\vartheta + \delta_n - \dot{\mathbf{x}}_{n_c} - \dot{\xi}_n\\
&= \mathbf{f}_n + \hat{\mathbf{B}}_n\mathbf{u}^0_c - \dot{\mathbf{x}}_{n_c} + \hat{\mathbf{B}}_n\left(\mathbf{u} - \mathbf{u}^0_c\right) + \left(\mathbf{B}_n - \hat{\mathbf{B}}_n\right)\mathbf{u} + \varphi_n^T\vartheta + \delta_n - \dot{\xi}_n\\
&= \mathbf{f}_n + \hat{\mathbf{B}}_n\alpha_n - \hat{\mathbf{B}}_n\mathbf{u}^T\kappa_u\mathbf{u}\mathbf{z}_n - \dot{\mathbf{x}}_{n_c} + \varphi_n^T\vartheta + \delta_n + C_n\xi_n + \left(\mathbf{B}_n - \hat{\mathbf{B}}_n\right)\mathbf{u}\\
&= -\left(C_n + S_n\right)\left(\mathbf{x}_n - \mathbf{x}_{n_c} - \xi_n\right) + \varphi_n^T\tilde{\vartheta} + \delta_n - \beta_n - \mathbf{B}_{n-1}^T\mathbf{z}_{n-1} - \kappa_u\mathbf{z}_n - K_n\mathbf{e}_n + \left(\mathbf{B}_n - \hat{\mathbf{B}}_n\right)\mathbf{u},
\end{aligned}
\tag{6}
$$

where $\tilde{\vartheta} = \vartheta - \hat{\vartheta}$, and $\hat{\vartheta}$ is the estimate of the unknown parameter vector. Now consider the Control Lyapunov Function (CLF) candidate

$$
\mathcal{V}(\mathbf{z}, \psi, \mathbf{e}) = \frac{1}{2}\sum_{i=1}^{n}\left(\mathbf{z}_i^T\mathbf{z}_i + \chi_i^T\Gamma_i^{-1}\chi_i + \mathbf{e}_i^T K_i\mathbf{e}_i\right) \tag{7}
$$

where $\chi_i = \psi_i - \psi_i^M, \psi_i^M = \max\left(\psi_i^\star, \psi_i^0\right)$. The time derivative of the CLF (7) along the solutions of Eqs.

Downloaded by TECHNISCHE UNIVERSITEIT DELFT on December 30, 2013 | http://arc.aiaa.org | DOI: 10.2514/6.2010-7857

(5)–(6) satisfies

$$
\begin{aligned}
\dot{\mathcal{V}} &= \mathbf{z}_1^T\left(-C_1\mathbf{z}_1 - K_1\mathbf{e}_1 - \varphi_1^T\kappa_1\varphi_1\mathbf{z}_1 + \mathbf{B}_1\mathbf{z}_2 + \varphi_1^T\tilde{\vartheta} + \delta_1 - \beta_1\right)\\
&\quad + \sum_{i=2}^{n-1}\mathbf{z}_i^T\left(-C_i\mathbf{z}_i - K_i\mathbf{e}_i - \varphi_i^T\kappa_i\varphi_i\mathbf{z}_i - \mathbf{B}_{i-1}\mathbf{z}_{i-1} + \mathbf{B}_i\mathbf{z}_{i+1} + \varphi_i^T\tilde{\vartheta} + \delta_i - \beta_i\right)\\
&\quad + \mathbf{z}_n^T\left(-C_n\mathbf{z}_n - K_n\mathbf{e}_n - \varphi_n^T\kappa_n\varphi_n\mathbf{z}_n - \mathbf{B}_{n-1}\mathbf{z}_{n-1} + \varphi_n^T\vartheta + \delta_n - \beta_n - \kappa_u\mathbf{z}_n + (\mathbf{B}_n - \hat{\mathbf{B}}_n)\mathbf{u}\right)\\
&\quad + \sum_{i=1}^{n}\chi_i^T\left(\omega_i z_i - \sigma_i(\psi_i - \psi_i^0)\right) + \sum_{i=1}^{n}\mathbf{z}_i^T K_i\mathbf{e}_i\\
&= -\sum_{i=1}^{n}\mathbf{z}_i^T C_i\mathbf{z}_i - \sum_{i=1}^{n}\mathbf{z}_i^T\varphi_i^T\kappa_i\varphi_i\mathbf{z}_i + \sum_{i=1}^{n}\varphi_i^T\tilde{\vartheta}\mathbf{z}_i + \sum_{i=1}^{n}(\delta_i - \beta_i)\mathbf{z}_i - \mathbf{z}_n^T\kappa_u\mathbf{z}_n + \mathbf{z}_n^T(\mathbf{B}_n - \hat{\mathbf{B}}_n)\mathbf{u}\\
&\quad + \sum_{i=1}^{n}\chi_i^T\left(\omega_i\mathbf{z}_i - \sigma_i(\psi_i - \psi_i^0)\right)\\
&= -\sum_{i=1}^{n}\mathbf{z}_i^T C_i\mathbf{z}_i - \sum_{i=1}^{n}\left(\varphi_i\mathbf{z}_i - \frac{1}{2}\kappa_i^{-1}\tilde{\vartheta}\right)^T\kappa_i\left(\varphi_i\mathbf{z}_i - \frac{1}{2}\kappa_i^{-1}\tilde{\vartheta}\right) + \sum_{i=1}^{n}\frac{1}{4}\tilde{\vartheta}^T\kappa_i^{-1}\tilde{\vartheta}\\
&\quad - \left(\mathbf{z}_n - \frac{1}{2}\kappa_u^{-1}\tilde{\mathbf{B}}_n\mathbf{u}\right)^T\kappa_u\left(\mathbf{z}_n - \frac{1}{2}\kappa_u^{-1}\tilde{\mathbf{B}}_n\mathbf{u}\right) + \frac{1}{4}\mathbf{u}^T\tilde{\mathbf{B}}_n^T\kappa_u^{-1}\tilde{\mathbf{B}}_n\mathbf{u}\\
&\quad + \sum_{i=1}^{n}\delta_i\mathbf{z}_i - (\psi_i^M)^T\omega_i\mathbf{z}_i - \frac{1}{2}\chi_i^T\sigma_i\chi_i - \frac{1}{2}(\psi_i - \psi_i^0)^T\sigma_i(\psi_i - \psi_i^0) + \frac{1}{2}(\psi_i^M - \psi_i^0)^T\sigma_i(\psi_i^M - \psi_i^0)\\
&\le -\sum_{i=1}^{n}\mathbf{z}_i^T C_i\mathbf{z}_i + \frac{1}{4}\sum_{i=1}^{n}\tilde{\vartheta}^T\kappa_i^{-1}\tilde{\vartheta} + \frac{1}{4}\mathbf{u}^T\tilde{\mathbf{B}}_n^T\kappa_u^{-1}\tilde{\mathbf{B}}_n\mathbf{u} + \frac{1}{2}\sum_{i=1}^{n}(\psi_i^M)^T\varsigma_i + (\psi_i^M - \psi_i^0)^T\sigma_i(\psi_i^M - \psi_i^0)
\end{aligned}
\tag{8}
$$

where a claim from Ref. 29 is used to bound parts due to the adaptive bounding of disturbances. The second and third terms at the last line of (8) are due to the nonlinear damping, the last two terms are due to the adaptive bounding. The result in (8) shows that the tracking error states and desired control input are bounded when the parameter estimation errors are bounded, and that the tracking error states converge exponentially to a positively invariant compact set. Using the results from Ref. 30 the robustness bounds of the controller can be derived. Tracking performance can be improved by either increasing the nonlinear damping gains and adaptive bounding update gains, or reducing the parameter estimation error using online identification. Suppose that (8) could be rewritten as

$$\dot{\mathcal{V}} \le -\mathbf{z}^T C_0\mathbf{z} + \frac{1}{4}\tilde{\vartheta}^T\kappa_0^{-1}\tilde{\vartheta} + \frac{1}{4}\mathbf{u}^T\tilde{\mathbf{B}}_n^T\kappa_u^{-1}\tilde{\mathbf{B}}_n\mathbf{u} + \Lambda$$

where

$$
\begin{aligned}
C_0 &= \min_{1\le i\le n} C_i,\\
\kappa_0 &= \left(\sum_{i=1}^{n}\kappa_i^{-1}\right)^{-1},\\
\Lambda &= \tfrac{1}{2}\left[(\psi^M)^T\varsigma + (\psi^M - \psi^0)^T\sigma(\psi^M - \psi^0)\right]
\end{aligned}
$$

and $\Lambda > 0$ since $\varsigma_i > 0, \psi_i^M > 0, \sigma > 0$ by their definitions. Therefore

$$\mathbf{z}^T C_0\mathbf{z} \ge \left[\frac{1}{4}\tilde{\vartheta}^T\kappa_0^{-1}\tilde{\vartheta} + \frac{1}{4}\mathbf{u}^T\tilde{\mathbf{B}}_n^T\kappa_u^{-1}\tilde{\mathbf{B}}_n\mathbf{u} + \Lambda\right]$$

implies that $\dot{\mathcal{V}} < 0$ and therefore gives an upper bound on the invariant compact set to which $\mathbf{z}$ will converge.

II.C. Nonlinear Swapping Filters

Similar to their use in linear modular designs the swapping filters are used as an analytical device which uses regressor filtering to account for the time-varying nature of the parameter estimates.[4,31] The filters transform a time-varying system into a static mapping, such that only state measurements are required and not their derivatives. Two types of nonlinear swapping can be applied, either to the tracking error system,

Downloaded by TECHNISCHE UNIVERSITEIT DELFT on December 30, 2013 | http://arc.aiaa.org | DOI: 10.2514/6.2010-7857

or to the system dynamics. In this work x-swapping filters are selected to achieve the greatest similarity to NDI with RLS estimation technique used in Ref. 10. Note that the function of this filter is not state estimation, but rather to extract the unknown dynamics from the state and control feedback. First rewrite the system (2) in the form

$$\dot{\mathbf{x}} = \mathbf{f}(\mathbf{x},\mathbf{u}) + \mathbf{F}^T(\mathbf{x},\mathbf{u})\vartheta + \Delta(t,\mathbf{x},\mathbf{u}) \tag{9}$$

where

$$\mathbf{f}(\mathbf{x},\mathbf{u}) = \begin{bmatrix} \mathbf{B}_1\mathbf{x}_2 + \mathbf{f}_1(\mathbf{x}_1) \\ \vdots \\ \mathbf{B}_{n-1}\mathbf{x}_n + \mathbf{f}_{n-1}(\mathbf{x}) \\ \mathbf{B}_{n_0}\mathbf{u} + \mathbf{f}_n(\mathbf{x}) \end{bmatrix}, \ \mathbf{F}^T(\mathbf{x},\mathbf{u}) = \begin{bmatrix} \varphi_1^T(\mathbf{x},\mathbf{u}) \\ \vdots \\ \varphi_{n-1}^T(\mathbf{x},\mathbf{u}) \\ \varphi_n^T(\mathbf{x},\mathbf{u}) \end{bmatrix}.$$

The x-swapping filters are applied

$$\dot{\Omega}_0 = A(t)(\Omega_0 + \mathbf{x}) - \mathbf{f}(\mathbf{x},\mathbf{u}), \ \Omega_0 \in \mathbb{R}^n \tag{10a}$$

$$\dot{\Omega}^T = A(t)\Omega^T + \mathbf{F}(\mathbf{x},\mathbf{u})^T, \qquad \Omega \in \mathbb{R}^{p\times n}. \tag{10b}$$

The matrix $A(t)$ is an exponentially stable matrix, that is a matrix with all eigenvalues in the left half plane, defined as

$$A(t) = A_0 - \rho\mathbf{F}^T\mathbf{F}P, \tag{11}$$

where $\rho > 0$ and A_0 is an arbitrary negative definite matrix such that

$$PA_0 + A_0^T P = -I, \ P = P^T > 0,$$

to stabilize the scheme against fast parameter and regressor variations. Since $A_0 < 0$, $rho > 0$, $P > 0$ and $\mathbf{F}^T\mathbf{F} > 0$, the matrix $A(t) < 0 \forall t$. For the identification algorithm discussed in the following section the output Ω is used as the regressor, and the output vector $\mathcal{Y} = \Omega_0 + \mathbf{x}$ as the dependent variable. The estimation error is defined as

$$\epsilon = \Omega_0 + \mathbf{x} - \Omega^T\tilde{\vartheta} \tag{12}$$

which satisfies

$$\epsilon = \Omega^T\tilde{\vartheta} + \tilde{\epsilon} \tag{13}$$

where $\tilde{\epsilon}$ is the filtered disturbance

$$\dot{\tilde{\epsilon}} = A(t)\tilde{\epsilon} + \Delta. \tag{14}$$

Since $A(t)$ is exponentially stable, and Δ is bounded, $\tilde{\epsilon}$ is bounded and even converges to zero exponentially for $\Delta = 0$. Therefore, ϵ is bounded, and converges to zero when $\Delta = 0$. Since ϵ is $\mathcal{L}_2$, $\mathbf{F}$ is smooth, and all states are bounded, $\ddot{\epsilon}$ is also bounded. Therefore, $\dot{\epsilon}$ is uniformly continuous. Since $\epsilon(t) \to 0$ for $\Delta = 0$, then

$$\lim_{t\to\infty}\int_0^t \dot{\epsilon}(\tau)d\tau = \lim_{t\to\infty}\epsilon(t) - \epsilon(0) = -\epsilon(0) < -\infty. \tag{15}$$

By Barbalat's lemma, $\dot{\epsilon}(t) \to 0$. Since $\dot{\tilde{\vartheta}} \in \mathcal{L}_\infty \cap \mathcal{L}_2$ and $\ddot{\tilde{\vartheta}} \in \mathcal{L}_\infty$, it hence follows that $\dot{\tilde{\vartheta}} \to 0$.

III. Full Envelope Model Identification

In the case that the on-board model is correct, the control law design from the previous section stabilizes the system, and achieves good tracking performance on the aircraft. Generally, the model used to predict the aerodynamic forces and moments is uncertain, or, in some flight conditions or failure conditions even unknown or unavailable. Therefore the on-board model is updated during the flight, to match the true aircraft behavior as close as possible. Since fighter aircraft dynamics vary nonlinearly through a large operating regime, the flight envelope is partitioned into small regions, which will be called hyperboxes. Each of these hyperboxes will contain a local linear-in-the-parameters-model. By combining the output of all of the local models together by means of smooth interpolation, a global nonlinear aerodynamic model is obtained. The main advantage of this approach is that the complexity of the local models can be relatively low, while still being able to obtain an accurate global approximation.

First of all the least squares method used to update the local models is discussed, after which the interpolation technique based on tensor B-splines is presented.

Downloaded by TECHNISCHE UNIVERSITEIT DELFT on December 30, 2013 | http://arc.aiaa.org | DOI: 10.2514/6.2010-7857

Downloaded by TECHNISCHE UNIVERSITEIT DELFT on December 30, 2013 | http://arc.aiaa.org | DOI: 10.2514/6.2010-7857

III.A. Local Model Update

The backstepping scheme introduced above can be combined by all identifiers which guarantee boundedness of the estimation error and its derivative. A Least Squares (LS) filter is selected here, since by design it can guarantee convergence of the parameter estimates to constant values. Instead of selecting an LS filter in combination within the modular backstepping framework applied in previous work,[24,32] an Orthogonal Least Squares (OLS) technique is applied to update the local models. The motivation for this is the planned extension towards online structure selection of the local linear models in future research. The current application of the OLS is equivalent to the continuous least squares formulation and therefore yields the same results. The continuous OLS description is started from the continuous time recursive least squares definition

$$\min_{\theta(t)} \int_0^t e^{\lambda(\tau-t)} \left(y(\tau) - \phi(\tau)^T \theta(t)\right)^2 d\tau \tag{16}$$

where the entries of $\phi(\tau) \in \mathbb{R}^p$ and $y(\tau)$ are given input signals, and the entries of $\theta(t) \in \mathbb{R}^p$ are unknown scalar constants. The scalar $\lambda \geq 0$ is a forgetting rate, determining the relative importance of the past input. Instead of directly solving this optimization problem, we perform a Cholesky factorization of the correlation matrix $\mathbf{N} = \langle \phi, \phi^T \rangle = \mathbf{R}^T \langle q, q^T \rangle \mathbf{R} = \mathbf{R}^T\mathbf{R}$, where $\mathbf{R}$ is the Cholesky factor of $\mathbf{N}$ and q is a vector of orthogonal vectors. Thus, (16) can now be rewritten as $\min_\theta \langle y, y \rangle - 2\langle y, \phi^T \rangle \theta + \theta^T \mathbf{N} \theta$, and the solution follows from $\mathbf{N}\theta = \langle \phi, y^T \rangle$, or $\mathbf{R}^T\mathbf{R}\theta = \mathbf{R}^T \langle q, y^T \rangle$. Therefore $\mathbf{R}$ and $\langle q, y^T \rangle$ need to be tracked. This can be achieved by adding an additional component to the input, $\hat{\phi} = \begin{bmatrix} \phi^T & y^T \end{bmatrix}^T$. However, instead of tracking the Cholesky factor $\hat{\mathbf{R}}$ of the augmented correlation matrix $\hat{\mathbf{N}}$, tracking the inverse Cholesky factor $\hat{\mathbf{S}} = \hat{\mathbf{R}}^{-1}$ allows extractionn the parameter estimate without matrix inversion or backsubstitution. From $\dot{\hat{\mathbf{N}}} = \hat{\phi}\hat{\phi}^T - \lambda\hat{\mathbf{N}}$ and the lemma which relates the evolution of a matrix and its Cholesky factor from Ref. 33 the following is obtained

$$\dot{\hat{\mathbf{S}}} = -\hat{\mathbf{S}} \ \text{upph}\left(\hat{\mathbf{S}}^T \hat{\phi}\hat{\phi}^T \hat{\mathbf{S}}\right) + \frac{\lambda}{2}\hat{\mathbf{S}} \tag{17}$$

where upph, the upper triangular half-part, is defined by

$$Y = \text{upph}(X) \iff \begin{cases} y_{i,j} = x_{i,j} & i < j \\ y_{i,j} = \frac{1}{2} x_{i,j} & i = j \\ y_{i,j} = 0 & i > j \end{cases} . \tag{18}$$

For the application with the backstepping control law designed earlier the input matrix becomes

$$\hat{\phi}^T = \begin{bmatrix} \Omega^T & (\Omega_0 + \mathbf{x}) \end{bmatrix} \tag{19}$$

The parameter estimate θ can be extracted easily by

$$\theta_i = -\hat{\mathbf{S}}_{i,p+1} / \hat{\mathbf{S}}_{p+1,p+1}. \tag{20}$$

The relation between the forgetting rate used in continous time and the more commonly known forgetting factor for discrete time is given by

$$T_s \lambda = -\ln \lambda_d, \tag{21}$$

where T_s is the sampling time of the discrete system, and λ_d is the discrete forgetting factor. For example, at a sampling rate of 50 Hz and a discrete forgetting factor of 0.98 the equivalent continous time forgetting rate is about 1.

Naturally, the parameters of the model cannot be accurately determined unless some conditions are imposed on the input signal. For adaptive control with online identification, convergence of the residual modeling error to zero is more important than convergence of the model parameters. When the input signal is persistently exciting (PE) the estimates will converge to constant values. By definition, ϕ satisfies a persistency of excitation condition if positive constants ρ_1, ρ_2 and T exist such that the following condition is satisfied $\forall t \geq 0$

$$\rho_1 I \leq \int_t^{t+T} \phi(\tau)\phi(\tau)^T d\tau \leq \rho_2 I. \tag{22}$$

The reference trajectory can be made PE by superimposing a sinusoidal signal on the reference signal, as discussed in Ref. 34. Another method is by using an intelligently exciting signal,[35,36] which decays with trajectory tracking and parameter estimation errors.

Downloaded by TECHNISCHE UNIVERSITEIT DELFT on December 30, 2013 | http://arc.aiaa.org | DOI: 10.2514/6.2010-7857

III.B. Full Envelope Interpolation

Naturally, the estimation method described previously could be used to fit a model to the complete dynamics of the aircraft. However, to be able to achieve a reasonably accurate fit throughout the whole flight envelope such a model would be extremely complex and large. For such a large model, the covariance matrix would become very large since its number of elements scales quadratically, increasing the computational load of the identification scheme dramatically. Therefore an approach is selected which splits the complete flight envelope into partitions, the output of the smaller partitions is combined using smooth interpolation functions. It is desired to only update the model in the *active* part of the flight envelope, and therefore interpolating functions with local support are selected: B-splines.

A B-spline is a spline function that has minimal support with respect to a given degree, smoothness and domain partition.[37]

Definition III.1 (B-spline basis function) *: Let U be a set of $m+1$ nondecreasing numbers, $u_0 \leq u_1 \leq \ldots \leq u_m$. The u_i are called knots, the set U the knot vector, and the half-open interval $[u_i, u_{i+1})$ the i^{th} knot span. If a knot u_i appears k times, where $k > 1$, u_i is a multiple knot of multiplicity k, written as $u_i(k)$. Otherwise it is called a simple knot. The knots can be considered as division points that subdivide the interval $[u_0, u_m]$ into knot spans. All B-spline basis functions are supposed to have their domain on $[u_0, u_m]$. To define B-spline basis functions one more parameter is required, the degree of these basis functions, p. The ith B-spline basis function of degree p, written as $N_{i,p}(u)$, is defined recursively as follows:*

$$
\begin{aligned}
F_{i,0}(u) &= \begin{cases} 1 & \text{if} \quad u_i \leq u < u_{i+1} \\ 0 & \text{otherwise} \end{cases} \\
F_{i,p}(u) &= \frac{u - u_i}{u_{i+p} - u_i} F_{i,p-1}(u) + \frac{u_{i+p+1} - u}{u_{i+p+1} - u_{i+1}} F_{i+1,p-1}(u)
\end{aligned}
$$

This formula is usually referred to as the Cox-de Boor recursion formula.

The B-splines have two characteristics that make them very suitable for online identification:

1. Only a small number of B-spline basis functions is nonzero at any given point in the flight envelope. Therefore only a small number of local models has to be updated, resulting in lower computational load. Additionally, since the update is local, the model has memory capabilities. Moving through the complete flight envelope model information is stored.

2. The spline output is always positive and normalized, resulting in a numerical stable process.

In Fig. 2(a) the output of a cubic B-spline network is shown, along with the individual B-splines and the control points. The B-spline is generalized for higher input dimensions by taking the tensor product of the B-spline basis functions in each of dimension, for example in three dimensions this yields

$$\gamma_{ijk} = \gamma_i \otimes \gamma_j \otimes \gamma_k. \tag{23}$$

Fig. 2(b) shows the degree of membership for a cubic B-spline basis function for two input dimensions with knot vectors $x_{knot} = y_{knot} = \begin{bmatrix} -2 & -2 & -2 & -2 & -1 & 0 & 1 & 2 & 2 & 2 & 2 \end{bmatrix}$. Note that the shape of the basis functions changes near the edges of the domain to keep the sum of all invidual degrees of membership equal to 1.

The degree of membership γ_i, the B-spline output, is used to distribute the current measurement over the active local models as a weight on their derivatve.

$$\dot{\hat{\mathbf{S}}}_i = -\hat{\mathbf{S}}_i \text{ upph}\left(\hat{\mathbf{S}}_i^T \hat{\phi} \gamma_i \hat{\phi}^T \hat{\mathbf{S}}_i\right) + \frac{\lambda \gamma_i}{2} \hat{\mathbf{S}}_i \tag{24}$$

For the inactive local models, with $\gamma_j = 0$

$$\dot{\hat{\mathbf{S}}}_j = 0. \tag{25}$$

The output at any given point in the flight envelope can be obtained by summing the weighted output of the local models as

$$\vartheta = \sum_i \gamma_i \vartheta_i \tag{26}$$

where ϑ_i is the output of the $i-$th local model.

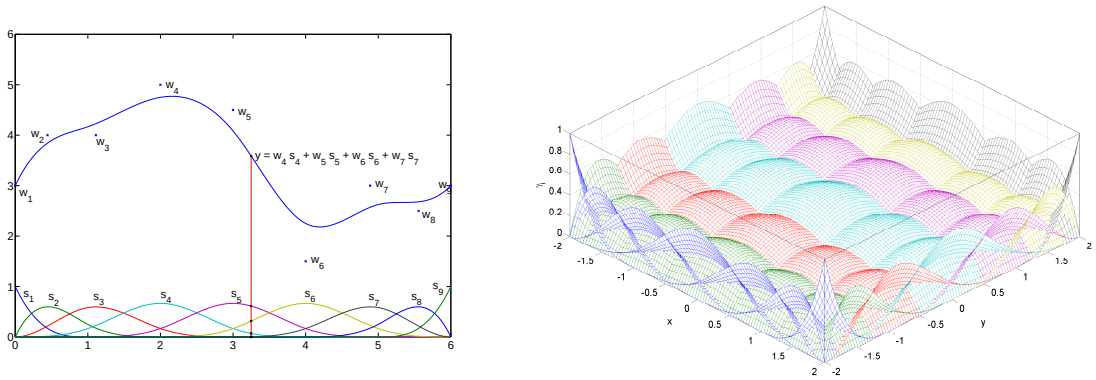

(a) (b)

Figure 2. A cubic B-Spline function output is shown in (a). The output at a given input point is the weighted sum of the active B-Splines. The Degree of local membership determined by cubic B-spline basis functions in two dimensions with knot vectors $x_{knot} = y_{knot} = [-2 \ -2 \ -2 \ -2 \ -1 \ 0 \ 1 \ 2 \ 2 \ 2 \ 2]$ is shown in (b).

III.C. Covariance Resetting

The covariance matrix generally becomes very small after a period of tracking without any noticeable mismatch between the on-board model and the true aircraft behaviour, despite using a forgetting factor in Eq. (24). This reduces the ability of the identifier to adjust to abrupt changes in the system dynamics. For aircraft, and especially fighter aircraft, slow adaptation to the new dynamics could cause the aircraft to reach dangerous or unrecoverable regions of the state space. Therefore, a mechanism is applied to reset the covariance matrix to enable fast adaptation when an abrupt change is detected. After a sudden change, the residual vector ϵ will in general be large. By monitoring the residual, and comparing it with a degree of membership weighted pre-defined threshold, abrupt changes can be detected and consequently reset the covariance matrix of that particular hyperbox, i.e.

$$|\epsilon| \geq \gamma_i W_\epsilon. \tag{27}$$

The trace of the inverse covariance matrix has to be below a certain threshold, to avoid repeated and continuous resetting after a failure. Note that the estimated parameters are not reset to zero, only their "update gain".

IV. Application to F-16 Model

The control design presented in the preceding sections is applied to a nonlinear model of the F-16 from Ref. 38. The aerodynamic data tables are valid in the subsonic regime, with an angle of attack between -20 and 90 degrees, and sideslip angle of $-30 \leq \beta \leq 30$ degrees. The tabular data in the model is obtained from wind-tunnel tests and captures the nonlinear behavior of the total aerodynamic force and moment coefficients. A quaternion representation of the attitude is used to avoid the 90 degree pitch singularity.

IV.A. F-16 Aircraft Model and Assumptions

The F-16 model allows for control over thrust-lever, horizontal stabilizer, ailerons, and rudder. Additionally the assumption is made that either thrust measurements or an accurate thrust model is available. The control inputs are defined positive in the conventional way: a positive control deflection results in a negative force or moment in the body-axes. The F-16 is equipped with automatic leading edge flaps, which are deflected according to a transfer function dependent on angle of attack α and a bias depending on the ratio of dynamic pressure and static pressure (Mach number)[38]

$$\delta_{LEF_c} = 1.38\frac{2s + 7.25}{s + 7.25}\alpha - 9.05\frac{\bar{q}}{p_{static}} + 1.45$$

The control surfaces of the F-16 are driven by servo-controlled actuators to produce the deflections commanded by the flight control system, u, which are the true control variables. The actuators of the

Downloaded by TECHNISCHE UNIVERSITEIT DELFT on December 30, 2013 | http://arc.aiaa.org | DOI: 10.2514/6.2010-7857

control surfaces are modeled as a first-order low-pass filters with fixed gain and saturation limits in range and deflection rate, see Table 1. The time constants of the actuators are 0.136 for the leading edge flaps and 0.0495 for the other control surfaces. The throttle response used in the F-16 is modeled as low-pass filter with time constant 1.0.

Table 1. The control input units and maximum values

Control	Unit	Min.	Max.	Rate limit
Thrust-lever	-	0	1	$\pm$ 5 s^{-1}
Horizontal Tail	deg	-25.0	25.0	$\pm$ 60 deg/s
Ailerons	deg	-21.5	21.5	$\pm$ 80 deg/s
Rudder	deg	-30.0	30.0	$\pm$ 120 deg/s
Leading edge flap	deg	0.0	25.0	$\pm$ 25 deg/s

The original nonlinear model is not affine in the control surface inputs, the horizontal stabilizer appears as an input to several lookup tables. Therefore an affine approximation of these tables is made, introducing an model-mismatch. For example, the moment coefficient C_m is approximated as

$$C_m(\alpha,\beta,\delta_e) \approx C_{m_0}(\alpha,\beta,\delta_e) + C_{m_{\delta_e}}(\alpha,\beta,\delta_e)\delta_{e_c} \tag{28}$$

since the current deflection δ_e is known through the command filters. This approximation is valid over a small range of elevator deflections around the current operating point. By partitioning on the stabilizer deflection, an accurate approximation is obtained for the full range of elevator deflections. Other similar coefficients which have a non-affine dependence on the stabilizer deflection are approximated similarly. This approximation does however create a mismatch between the true aircraft dynamics and the modeled aircraft dynamics, thereby introducing an unknown disturbance which is modeled as δ in Eq. (2). Using the adaptive bounding technique, the controller is robustified against this unknown model mismatch.

IV.B. Partition Model Structure

The incremental model estimated on-board the aircraft is based on the linearized system equations.[39] The local models of the different hyperboxes is not necesarily the same: for example partitions at extreme angles of attack and sideslip angles can have a more complex model structure to capture all the nonlinear phenomena occurring. In this work the following local model structure has been selected for all hyperboxes

$$\begin{aligned}
\delta C_X &= \begin{bmatrix} 1 & \frac{q\bar{c}}{2V_T} & \delta_e \end{bmatrix} \begin{bmatrix} \delta C_{X_0} & \delta C_{X_q} & \delta C_{X_{\delta_e}} \end{bmatrix}^T, \\
\delta C_Y &= \begin{bmatrix} 1 & \frac{pb}{2V_T} & \frac{rb}{2V_T} & \delta_a & \delta_r \end{bmatrix} \begin{bmatrix} \delta C_{Y_0} & \delta C_{Y_p} & \delta C_{Y_r} & \delta C_{Y_{\delta_a}} & \delta C_{Y_{\delta_r}} \end{bmatrix}^T, \\
\delta C_Z &= \begin{bmatrix} 1 & \frac{q\bar{c}}{2V_T} & \delta_e \end{bmatrix} \begin{bmatrix} \delta C_{Z_0} & \delta C_{Z_q} & \delta C_{Z_{\delta_e}} \end{bmatrix}^T, \\
\delta C_l &= \begin{bmatrix} 1 & \frac{pb}{2V_T} & \frac{rb}{2V_T} & \delta_a & \delta_e & \delta_r \end{bmatrix} \begin{bmatrix} \delta C_{l_0} & \delta C_{l_p} & \delta C_{l_r} & \delta C_{l_{\delta_a}} & \delta C_{l_{\delta_e}} & \delta C_{l_{\delta_r}} \end{bmatrix}^T, \\
\delta C_m &= \begin{bmatrix} 1 & \alpha & \frac{q\bar{c}}{2V_T} & \delta_e \end{bmatrix} \begin{bmatrix} \delta C_{m_0} & \delta C_{m_\alpha} & \delta C_{m_q} & \delta C_{m_{\delta_e}} \end{bmatrix}^T, \\
\delta C_n &= \begin{bmatrix} 1 & \frac{pb}{2V_T} & \frac{rb}{2V_T} & \delta_a & \delta_e & \delta_r \end{bmatrix} \begin{bmatrix} \delta C_{n_0} & \delta C_{n_p} & \delta C_{n_r} & \delta C_{n_{\delta_a}} & \delta C_{n_{\delta_e}} & \delta C_{n_{\delta_r}} \end{bmatrix}^T.
\end{aligned} \tag{29}$$

The regressor functions are block-diagonally stacked together to form the full regressor matrix, all the incremental unknown parameters are stacked to form a large column-vector with 27 parameters.

IV.C. F-16 Control Law Design

The controller design discussed in the previous sections is applied to the F-16 aircraft model. The application of the proposed control scheme is not presented in great detail since it is very similar to earlier work found in Refs. 14, 40. A tracking controller for the total airspeed, angle of attack, sideslip angle, and velocity vector roll rate is designed.

Downloaded by TECHNISCHE UNIVERSITEIT DELFT on December 30, 2013 | http://arc.aiaa.org | DOI: 10.2514/6.2010-7857

Downloaded by TECHNISCHE UNIVERSITEIT DELFT on December 30, 2013 | http://arc.aiaa.org | DOI: 10.2514/6.2010-7857

First define the outer loop subsystem as

$$\mathbf{x}_1 = \begin{bmatrix} V_T & \alpha & \beta \end{bmatrix}^T \tag{30}$$

with dynamics

$$\dot{\mathbf{x}}_1 = \mathbf{f}_1 + \mathbf{F}_1 + \mathbf{B}_1 \begin{bmatrix} p_S & q_S & r_S \end{bmatrix}^T + \mathbf{B}_{1_T} \begin{bmatrix} T & 0 & 0 \end{bmatrix}^T \tag{31}$$

where

$$\mathbf{f}_1 = \begin{bmatrix} g_1 \\ -p_S \tan\beta + \dfrac{1}{mV_T \cos\beta}\left(-T\sin\alpha + mg_3\right) \\ \dfrac{1}{mV_T}\left(-T\cos\alpha\sin\beta + mg_2\right) \end{bmatrix},$$

$$\mathbf{F}_1 = \frac{1}{m}\begin{bmatrix} -\cos\alpha\cos\beta & \sin\beta & \sin\alpha\cos\beta \\ -\dfrac{\sin\alpha}{V_T\cos\beta} & 0 & \dfrac{\cos\alpha}{V_T\cos\alpha} \\ -\dfrac{\cos\alpha\sin\beta}{V_T} & \dfrac{\cos\beta}{V_T} & -\dfrac{\sin\alpha\sin\beta}{V_T} \end{bmatrix}\begin{bmatrix} \bar{X} \\ \bar{Y} \\ \bar{Z} \end{bmatrix},$$

$$\mathbf{B}_1 = \begin{bmatrix} 0 & 0 & 0 \\ 0 & 1 & 0 \\ 0 & 0 & -1 \end{bmatrix}, \quad \mathbf{B}_{1_T} = \begin{bmatrix} \dfrac{\cos\alpha\cos\beta}{m} & 0 & 0 \\ 0 & 0 & 0 \\ 0 & 0 & 0 \end{bmatrix}.$$

Note that this differs slightly from the system description given by (2) due to the presence of the control input T. The thrust input can be obtained from this outer loop for airspeed control. For the inner loop subsystem state is

$$\mathbf{x}_2 = \begin{bmatrix} p_S & q_S & r_S \end{bmatrix}^T \tag{32}$$

with dynamics

$$\dot{\mathbf{x}}_2 = \mathbf{f}_2 + \mathbf{F}_2 + \mathbf{B}_2 \begin{bmatrix} \delta_a & \delta_e & \delta_r \end{bmatrix}^T$$

where

$$\mathbf{f}_2 = -T_{B\to S}\mathbf{J}^{-1}\left(\omega_B \times \mathbf{J}\omega_B\right) + \dot{T}_{B\to S}\omega_B,$$

$$\mathbf{F}_2 = T_{B\to S}\mathbf{J}^{-1}\begin{bmatrix} L_0 \\ M_0 \\ N_0 \end{bmatrix},$$

$$\mathbf{B}_2 = T_{B\to S}\mathbf{J}^{-1}\begin{bmatrix} L_{\delta_a} & L_{\delta_e} & L_{\delta_r} \\ 0 & M_{\delta_e} & 0 \\ N_{\delta_a} & N_{\delta_e} & N_{\delta_r} \end{bmatrix}.$$

The aerodynamic forces and moments appearing in the above equations in the design are split into a part that is assumed known, or the nominal model, and a contribution from the estimated incremental on-board model. For example, the total aerodynamic force in x-body direction can be written as

$$\bar{X} = \bar{q}S\left(\underbrace{C_X + C_{X_q}\frac{q\bar{c}}{2V_T}}_{\text{nominal}} + \underbrace{\delta C_{X_0} + \delta C_{X_q}\frac{q\bar{c}}{2V_T} + +\delta C_{X_{\delta_e}}\delta_e}_{\text{incremental}}\right). \tag{33}$$

Thus known nonlinearities from aerodynamics and inertia coupling, are included in the function $\mathbf{f}_1, \mathbf{f}_2$. The functions F_1 and F_2 define an incremental (nonlinear) aerodynamical model. The matrix B_2 defines the aerodynamic control effectiveness and is composed out of a known part, and an incremental part.

Downloaded by TECHNISCHE UNIVERSITEIT DELFT on December 30, 2013 | http://arc.aiaa.org | DOI: 10.2514/6.2010-7857

V. Simulation Scenarios and Results

This section presents the numerical simulation results from the application of the complete control design to the F-16 model of the previous section for a number of failure scenarios and flight conditions. The controller is evaluated on tracking performance and estimation accuracy. The control design has been implemented in the MATLAB/Simulink© environment by means of S-functions written in C++. First the tuning of the design will be discussed, followed by an introduction of the failure scenarios and flight conditions. After this, the simulations results will be presented and discussed. The simulations performed run in real time on a 2.4 Ghz desktop machine.

V.A. Controller Tuning

First of all the command shaping filters, see Fig. 1, are discussed. The purpose of the filters is to transform step-like input signals from the pilot or outer-loop flight path controller to smooth reference signals as input to the controller. These filters can be tuned and scheduled such that level 1 handling qualities can be achieved through the whole flight envelope, by scheduling their tuning on the flight conditions. In this work a single tuning is selected for the whole flight envelope to simplify the design, since the main focus is on the feasibility of the control law design with online incremental model identification. The command filters are second-order low pass filters with magnitude constraints, the dynamics of these filters are

$$\begin{bmatrix} \dot{x}_c(t) \\ \ddot{x}_c(t) \end{bmatrix} = \begin{bmatrix} q_1 \\ q_2 \end{bmatrix} = \begin{bmatrix} q_2 \\ 2\zeta\omega_n \left[S_R \left(\frac{\omega_n^2}{2\zeta\omega_n} \left[S_M(x^0) - q_1 \right] \right) - q_2 \right] \end{bmatrix} \tag{34}$$

where $S_M(\cdot)$ and $S_R(\cdot)$ represent the magnitude and rate limit functions respectively. The tuning parameters for the filters are shown in Table 2. The Lyapunov design only requires the controller gains to be negative definite, but it is more natural to select the inner loop gains higher than the outer loop gains to achieve good tracking performance. The controller tracking error gains are selected as,

$$C_1 = \begin{bmatrix} 0.5 & 0 & 0 \\ 0 & 0.5 & 0 \\ 0 & 0 & 0.5 \end{bmatrix}, \; C_2 = \begin{bmatrix} 1.5 & 0 & 0 \\ 0 & 1.0 & 0 \\ 0 & 0 & 1.0 \end{bmatrix}$$

and the integrated tracking error gain only on the integrated stability axis roll rate

$$K_1 = \begin{bmatrix} 0 & 0 & 0 \\ 0 & 0 & 0 \\ 0 & 0 & 0 \end{bmatrix}, \; K_2 = \begin{bmatrix} 0.25 & 0 & 0 \\ 0 & 0 & 0 \\ 0 & 0 & 0 \end{bmatrix}.$$

Table 2. Command filter parameters.

Variable	Bandwidth	Damping	Magnitude Constraints
V_T	0.2	1.0	-
α	1.5	$\sqrt{2}/2$	-
β	2.0	$\sqrt{2}/2$	-
p_s	2.0	$\sqrt{2}/2$	-
q_s	100	$\sqrt{2}/2$	± 50 deg/s
r_s	100	$\sqrt{2}/2$	± 15 deg/s

The nonlinear damping gains κ are tuned to small values, if the parameter estimation is fast and accurate their contribution to the tracking performance is small. Therefore they are selected as $0.01I$ with I the identity matrix of appropriate size. The adaptive bounding gains are chosen small too since the assumption is made that the local model structure and the flight envelope partitioning will result in an accurate incremental

model. The update gain Γ and leakage term σ are selected as

$$\Gamma = \text{diag}\left(\left[\begin{array}{cccccc} 1\times10^{-6} & 1\times10^{-1} & 1\times10^{-1} & 1\times10^{-1} & 1\times10^{-1} & 1\times10^{-1} \end{array}\right]\right)$$

$$\sigma = 1\times10^{-1}I_6$$

The nonlinear swapping tuning parameters are selected such that the relevant dynamics of the aircraft can be captured. The swapping filter matrix is chosen as $A_0 = -100I_6$ and the damping gain $\rho = 0.01$. The flight envelope is partitioned in three dimensions for the incremental model: the angle of attack, the sideslip angle, and horizontal stabilizer deflection, equivalent to most lookup tables in the existing model. Each input dimension of the B-spline basis functions is partitioned uniformly since this resulted in good tracking performance in earlier work.[14] The flight envelope partitioning is defined in Table 3. The number of hyperbox partitions is a tradeoff between local model complexity, required onboard storage capacity, and model accuracy. The order of the B-spline interpolation functions is a tradeoff between the smoothness of the estimated model, and the number of active local models. Second order B-splines are used for all the input dimensions, since this produces a smooth nonlinear model, while limiting the number of active local models at any given point in the flight envelope to $3\times3\times3 = 27$.

Table 3. Flight envelope partitioning

Variable	min. (deg)	max. (deg)	step (deg)	hyperbox partitions
Angle of attack	-20	90	5	24
Sideslip angle	-30	30	5	14
Horizontal stabilizer deflection	-25	25	5	12
Total				4032

A very mild forgetting rate of $\lambda = 0.005$ has been selected for all the partitions, this would correspond to a discrete forgetting factor of 0.9999 at 50 Hz sampling. The partitions are initialized with small values of the Cholesky factor of the covariance matrix, and a reset is triggered when an element of the partitition weighted absolute estimation error vector exceeds

$$W_\epsilon = 1\times10^{-6}\left[\begin{array}{cccccc} 1 & 1 & 1 & 1 & 1 & 1 \end{array}\right]^T$$

the Cholesky factor for that particular partition is reset to

$$\hat{\mathbf{S}}_{\text{reset}} = \text{diag}\left(\left[\begin{array}{cccccccccccccc} 10^2 & 10^4 & 10^3 & 10^2 & 10^2 & 10^2 & 10^3 & 10^3 & 10^2 & 10^3 & 10^3 & 10^2 & 10^2 & 10^2 \\ 10^4 & 10^4 & 10^4 & 10^2 & 10^3 & 10^5 & 10^3 & 10^2 & 10^2 & 10^2 & 10^4 & 10^4 & 10^4 & 1 \end{array}\right]\right)$$

to encourage fast adaptation to the changed system dynamics.

V.B. Simulation Scenarios

Three types of simulation scenarios are defined, the nominal case for which no faults occur, secondly a scenario where the center of gravity suddenly shifts in longitudinal direction, and finally scenarios in which the right aileron surface moves to a specified position and locks up..All simulations last 60 seconds. The simulations have been performed at two flight conditions, one at low altitude, 1000m at Mach 0.3, the other at cruise altitude of 10000m and Mach 0.8. Since the aircraft's maneuverability is different at these flight conditions, also different maneuvers have been performed at these flight conditions. In Fig. 3 the input commands for the two flight conditions is shown.

The aileron faults are introduced after 7 seconds in the simulation, and the occur when the aircraft is roll and pitching simultaneously. Three different lock positions are considered: locking at zero-deflection, lock at half deflection of 10.75 degrees, and a lock at full deflection or full hard-over of 21.5 degrees. Note that this aircraft model does not contain a differential stabilizer inputs, hence only the rudder and the left aileron can be used to compensate the roll moment disturbance in this fault scenario.

Downloaded by TECHNISCHE UNIVERSITEIT DELFT on December 30, 2013 | http://arc.aiaa.org | DOI: 10.2514/6.2010-7857

Downloaded by TECHNISCHE UNIVERSITEIT DELFT on December 30, 2013 | http://arc.aiaa.org | DOI: 10.2514/6.2010-7857

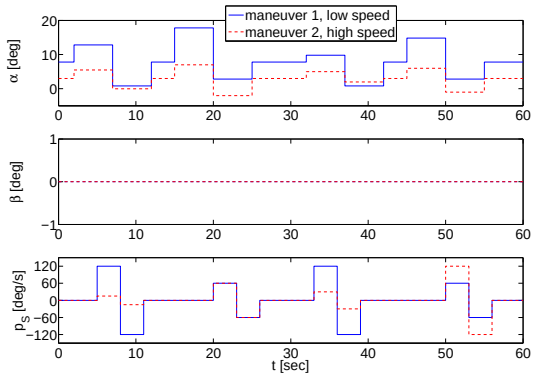

Figure 3. Input commands for the different maneuvers at different flight conditions.

In the last type of scenarios the center of gravity is suddenly shifted by 5% of the mean aerodynamic chord in longitudinal direction after 6 seconds into the simulation, which results in a change of longitudinal stability of the aircraft.

V.C. Simulation Results

First the nominal simulation results are presented to show that when the on-board model is accurate, excellent tracking performance of the angle of attack, sideslip angle, and velocity vector roll rate is achieved and the estimated incremental model paremeters are practically zero. Figure 4 shows the tracking response and tracking errors, and Fig. 5 shows the estimated local model parameters during the maneuvers. Tracking of the velocity command is difficult due to the relatively slow response of the engine compared to the dynamics of the aircraft. Additionally, it is not possible to give negative thrust and speedbrakes are not included in the model. When there is no change of the onboard dynamics, the identifier does not estimate a noticeable change in the incremental model parameters, and tracking performance is excellent for both flight conditions and maneuvers.

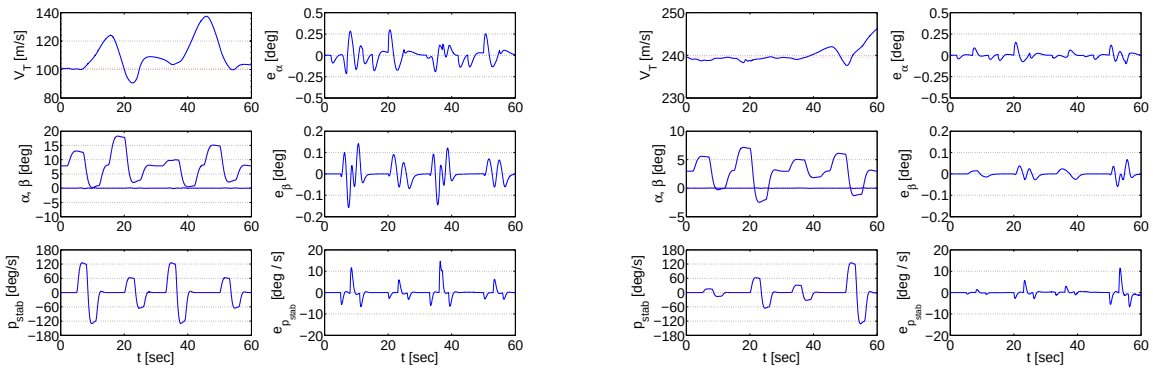

(a) (b)

Figure 4. Tracking response for two different maneuvers executed at two different flight conditions. Fig. 4(a) shows the tracking response for the low altitude, slow flight. Fig. 4(b) shows the tracking response for the cruise altitude and velocity.

A more demanding and interesting scenario for the proposed adaptive controller is a sudden shift of the center of gravity in longitudinal direction. The pitching and yawing coefficients will change as a result of this shift according to

$$\Delta C_m = C_Z \Delta x_{cg} \bar{c}$$
$$\Delta C_n = C_Y \Delta x_{cg} \frac{\bar{c}}{b}$$

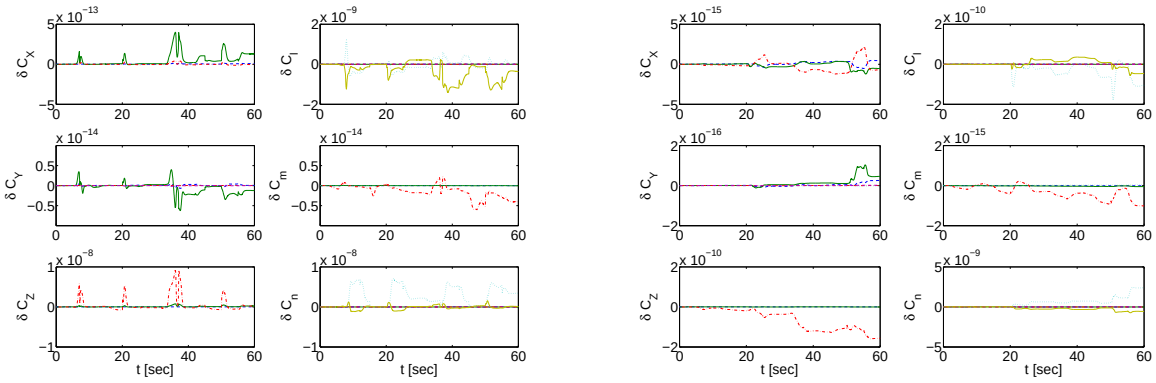

(a) (b)

Figure 5. Incremental model parameters estimated during the nominal tracking maneuvers at two different flight conditions. Fig. 5(a) shows the tracking response for the low altitude, slow flight. Fig. 5(b) shows the tracking response for the cruise altitude and velocity.

where Δx_{cg} is the shift in longitudinal direction in percentage of the chord length, ΔC_m is the increment in pitch moment coefficient, and ΔC_n the increment in yaw moment coefficient. No inertia model was available, therefore the mass and moments of the aircraft do not change. Normally, aircraft are designed for a range of possible center of gravity positions. Especially for model based controllers a *known* change of position is therefore not a problem, a sudden unknown change on the other hand can cause degraded tracking performance and even stabilty problems. Figure 6(a) shows the tracking performance for a destabilizing shift of 5% of the mean aerodynamic chord, or 0.1725 m. In Fig. 6(b) the control deflections are compared with the nominal center of gravity position deflections. Figure 7(a) shows the response and tracking error of the proposed control scheme without any adaptation, i.e. $\hat{\theta} = 0, \psi = 0$. Clearly the tracking performance has decreased a lot caused by the mismatch between the onboard model and the true aircraft dynamics.

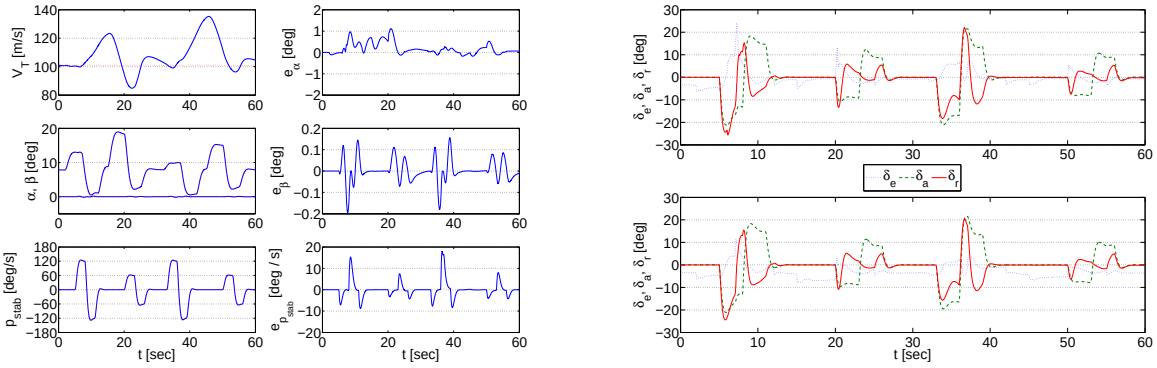

(a) (b)

Figure 6. Figure 6(a) shows the response of the aircraft for a sudden center of gravity shift after 6 seconds at low altitude, low speed flight. Figure 6(b) shows the control surface deflections for the shifted center of gravity location at the top, and the nominal deflections the bottom.

The filtered residual error signals (14) are shown in Fig. 8 which shows that when a new part of the flight envelope is visited after the failure, first the filtered residuals increase after which they converge back to zero when the estimates for the active partitions are updated. The estimated incremental model parameters during the simulation are shown in Fig. 9(a). The failure is detected very rapidly, as seen in Fig. 9(b), and several of the active partitions are reset almost immediately. When a different part of the flight envelope is visited during the maneuvering, also the partitions that become active and have not been updated yet, are reset. To show that the update is only local, Fig. 10 shows the estimated δC_m at the end of the simulation compared to a cross-section of the interpolated lookup table value $C_Z(\alpha, \beta, \delta_e)$ at $\beta = 0$, which is a main contributor to the effect of the center of gravity shift. The figure clearly shows that the identifier only

Downloaded by TECHNISCHE UNIVERSITEIT DELFT on December 30, 2013 | http://arc.aiaa.org | DOI: 10.2514/6.2010-7857

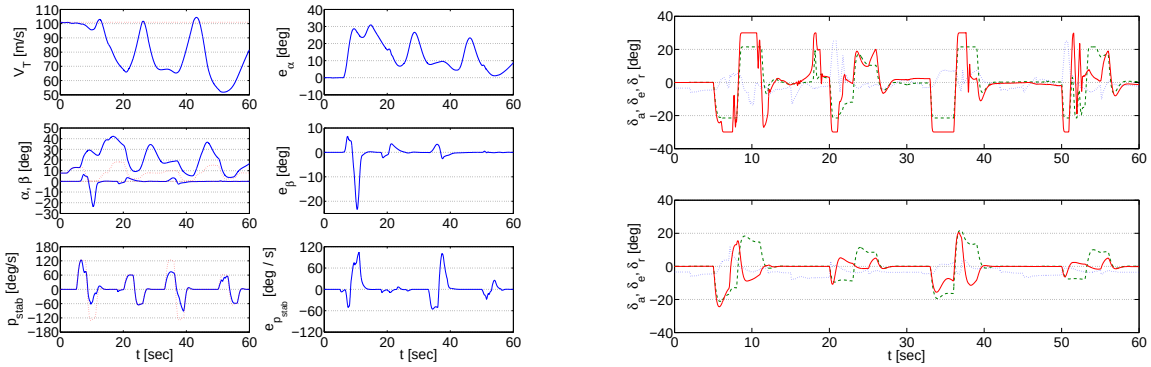

(a) (b)

Figure 7. Fig. 7(a) shows the response and tracking errors of the aircraft with non-adaptive controller for a sudden center of gravity shift after 6 seconds at low altitude, low speed flight. Figure 7(b) shows the difference between the control deflections for the aircraft with changed c.g. location (top) and the nominal position (bottom).

estimated in the part of the envelope where the aircraft has flown, and that the estimation is accurate.

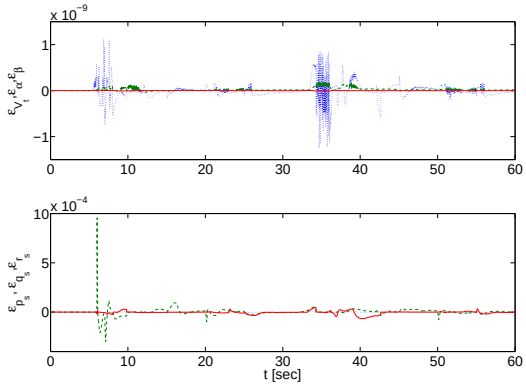

Figure 8. The filtered resiudals for the adaptive controller for a sudden center of gravity shift after 6 seconds.

The proposed control design with a single partition, i.e. one local model, for the whole flight envelope has been simulated. The tracking performance of the controller is of the same level as the partitioned controller as shown in Figure 11, the scheme has less capability however to store its estimated data for different parts of the flight envelope. Although the single incremental model control design is capable of approximating the incremental dynamics accurate over a limited portion of the flight envelope, it will never yield a globally valid approximation using the same model structure as for each of partitions of the fully partitioned flight envelope. This limitation is illustrated in Fig. 10, the single partition controller achieves a good approximation of δC_m for a small portion of the complete envelope: it fits a tangent plane to the true function. The fully partitioned envelope only approximates accurately in the visited part of the flight envelope, and its estimate in the unvisited parts is equal to zero. Increasing the order and complexity of the regressor would increase the approximation capabilities of the identifier in the single partitioned case. Unfortunately, it is not always clear which basis functions to include in the model such that the basis functions have physical interpretation, and increase the approximation capabilities.

Finally the results of one of the aileron experiments are shown: the case with a full hard-over of the right aileron at the cruise altitude and velocity. The response is shown in Fig. 12(a). Due to the reduced control authority around the longitudinal axis, the aircraft is not able to track the roll command, tracking of the angle of attack command is excellent however. Additionally, despite the locked aileron, the sideslip angle is very small in the order of a half degree. The estimated incremental model parameters are shown in Fig. 13(a). Clearly the change in dynamics is detected, and the identifier estimates mainly in the lateral directions. However, the incremental model estimates do not yet converge to their true values, not enough

Downloaded by TECHNISCHE UNIVERSITEIT DELFT on December 30, 2013 | http://arc.aiaa.org | DOI: 10.2514/6.2010-7857

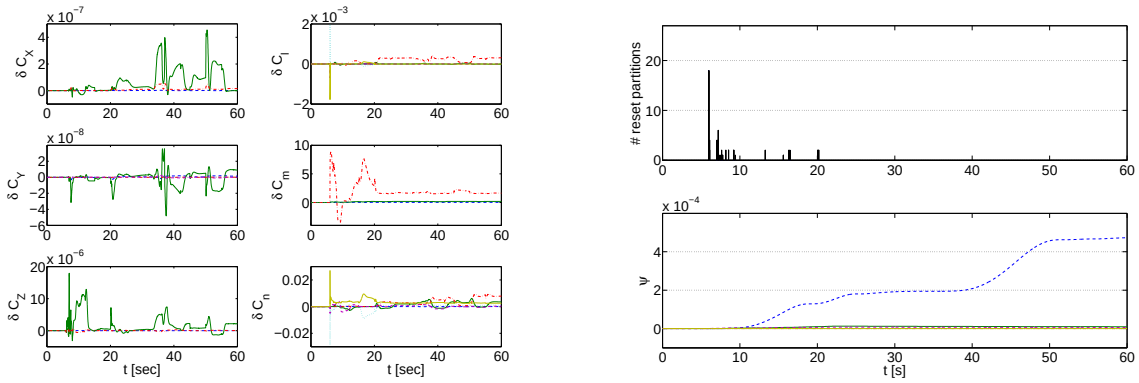

(a) (b)

Figure 9. Figure 9(a) shows the estimated incremental model parameters. Figure 9(b) shows the number of partitions reset at a certain time instant at the top, and at the bottom shows the adaptive bounding estimate ψ.

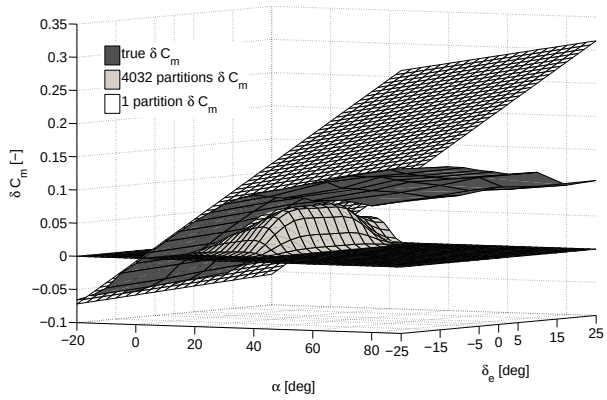

Figure 10. A 3d-view of an intersection at $\beta = 0$ of the estimated δC_m due to a change in the center of gravity position for a fully partitioned flight envelope, a single partition flight envelope, and the true change of the C_m coefficient caused by this shift.

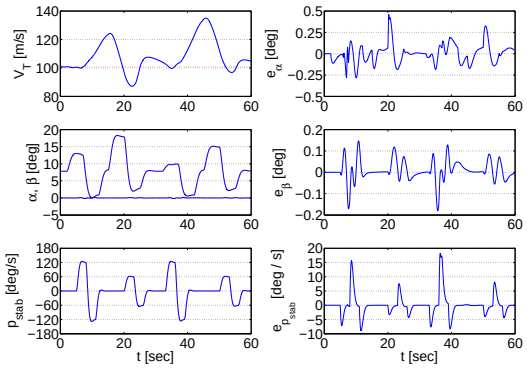

Figure 11. Response and tracking error of the adaptive controller with single partition incremental model for a sudden center of gravity shift after 6 seconds at low altitude, low speed flight.

Downloaded by TECHNISCHE UNIVERSITEIT DELFT on December 30, 2013 | http://arc.aiaa.org | DOI: 10.2514/6.2010-7857

information to estimate the correct parameters can be obtained from the flown maneuver. The control surface deflections are compared to the nominal case in Fig. 12(b).

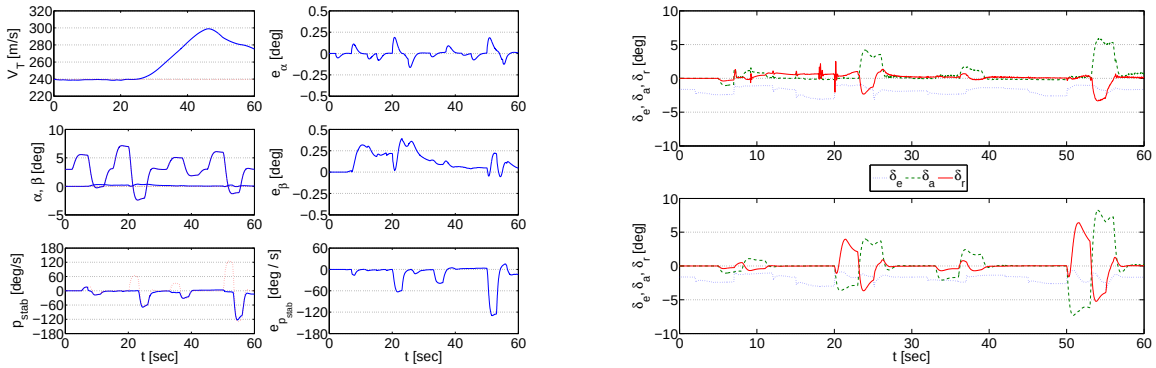

(a) (b)

Figure 12. Figure 12(a) shows the response of the aircraft after a full right aileron hardover at 7 seconds at high altitude, cruise speed flight. Figure 12(b) shows the control surface deflections for the aircraft with full right aileron hard-over at the top, and the nominal deflections the bottom.

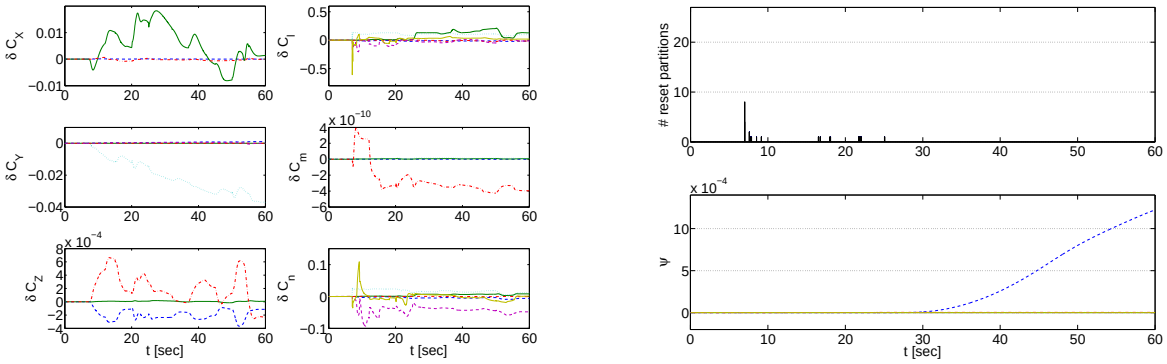

(a) (b)

Figure 13. Figure 13(a) shows the estimated incremental model parameters. Figure 13(b) shows the number of partitions reset at a certain time instant at the top, and at the bottom shows the adaptive bounding estimate ψ.

VI. Conclusions

In this paper a modular control design is presented for a high-fidelity nonlinear F-16 model. The controller is based on the backstepping approach, combined with a orthogonal least squares identifier. The flight envelope is partitioned into hyperboxes, in each of these hyperboxes a local linear-in-the-parameters model is estimated, and using second-order B-spline interpolation a smooth model is obtained for the complete flight envelope. To evaluate the tracking and estimation performance of the proposed adaptive design three types of scenario's were simulated. In the nominal scenario the controller showed very good tracking performance during simultaneous longitudinal and lateral maneuvering, while no change in incremental model was estimated. Furthermore, for simulation scenarios with a sudden change of longitudinal center of gravity position, tracking performance remained very good, and the correct change in aircraft dynamics was estimated. This scenario resulted in degradation of tracking performance for a non-adaptive controller. Finally, simulations with the right aileron locked at its maximum deflection showed that longitudinal tracking remained very good, while lateral tracking is restored partially after failure. Future research directions include online insertion, merging, and deletion of partitions and local model structure selection for each hyperbox.

Downloaded by TECHNISCHE UNIVERSITEIT DELFT on December 30, 2013 | http://arc.aiaa.org | DOI: 10.2514/6.2010-7857

Downloaded by TECHNISCHE UNIVERSITEIT DELFT on December 30, 2013 | http://arc.aiaa.org | DOI: 10.2514/6.2010-7857

References

[1]Shin, Y., Calise, A. J., and Johnson, M. D., "Adaptive Control of Advanced Fighter Aircraft in Nonlinear Flight Regimes," *Journal of Guidance, Control, and Dynamics*, Vol. 31, No. 5, 2008, pp. 1464 – 1477.

[2]Slotine, J. J. E. and Li, W., *Applied Nonlinear Control*, Prentice Hall, 1991, pp. 204,206–271.

[3]Isidori, A., *Nonlinear Control Systems*, Springer, 3rd ed., 1995, pp. 137 – 183, 227–262.

[4]Krstić., M. and Kokotović, P. V., "Adaptive Nonlinear Design with Controller-Identifier Separation and Swapping," *IEEE Transactions on Automatic Control*, Vol. 40, No. 3, March 1995, pp. 426 – 441.

[5]Krstić, M., Kanellakopoulos, I., and Kokotović, P. V., *Nonlinear and Adaptive Control Design*, Adaptive and Learning Systems for Signal Processing, John Wiley & Sons, Inc., 1995.

[6]Monopoli, R. V., "Model reference adaptive control with an augmented error signal," *Automatic Control, IEEE Transactions on*, Vol. 19, No. 5, 1974, pp. 474 – 484.

[7]Landau, I. D. and Courtiol, B., "Design of multivariable adaptive model following control systems," *Automatica*, Vol. 10, No. 5, 1974, pp. 483 – 494.

[8]Khalil, H. K., *Nonlinear Systems*, Vol. third edition, Prentice Hall, 2002, pp. 551 – 579, 611.

[9]Edwards, C. and Spurgeon, S., *Sliding Mode Control: Theory and Applications*, Taylor and Francis, Washington, D.C., 1998, pp. 31 – 34, 65.

[10]Lombaerts, T., Huisman, H., Chu, Q. P., Mulder, J. A., and Joosten, D., "Nonlinear Reconfiguring Flight Control based on Online Physical Model Identification," *Journal of Guidance, Control, and Dynamics*, Vol. 32, No. 3, 2009, pp. 727 – 748.

[11]Calise, A. J., Lee, S., and Sharma, M., "Development of a Reconfigurable Flight Control Law for Tailless Aircraft," *Journal of Guidance, Control and Dynamics*, Vol. 24, No. 5, Sep.-Oct. 2001.

[12]Singh, S. and Steinberg, M., "Adaptive Control of Feedback Linearizable Nonlinear Systems with Applicationto Flight Control," *AIAA Journal of Guidance, Control, and Dynamics*, Vol. 19, 1996, pp. 871 – 877.

[13]McFarland, M. B. and Calise, A. J., "Multilayer neural networks and adaptive nonlinear control of agile anti-air missiles," *AIAA Guidance, Navigation, and Control Conference*, AIAA, Reston, VA, August 1997, pp. 401 – 410.

[14]Sonneveldt, L., Chu, Q. P., and Mulder, J. A., "Nonlinear Flight Control Design using Constrained Adaptive Backstepping," *Journal of Guidance, Navigation, and Dynamics*, Vol. 30, No. 2, March - April 2007, pp. 322 – 336.

[15]Farrell, J., Sharma, M., and Polycarpou, M., "Backstepping Based Flight Control with Adaptive Function Approximation," *AIAA Journal of Guidance, Control and Dynamics*, Vol. 28, No. 6, Jan. 2005, pp. 1089 – 1102.

[16]Sharma, M. and Ward, D. G., "Flight-path angle control via neuro-adaptive backstepping," *AIAA Guidance, Navigation, and Control Conference and Exhibit*, Monterey, CA, Aug. 2002.

[17]Pashilkar, A. A., Sundararajan, N., and Saratchandran, P., "Adaptive Nonlinear Neural Controller for Aircraft Under Actuator Failures," *Journal of Guidance, Control, and Dynamics*, Vol. 30, No. 3, 2007, pp. 835 – 846.

[18]Shin, D. H. and Kim, Y., "Nonlinear Discrete-Time Reconfigurable Flight Control Law Using Neural Networks," *IEEE Transactions on Control Systems Technology*, Vol. 14, No. 3, May 2006, pp. 408 – 422.

[19]Nguyen, N., Krishnakumar, K., Kaneshige, J., and Nespeca, P., "Flight Dynamics and Hybrid Adaptive Control of Damaged Aircraft," *Journal of Guidance, Control, and Dynamics*, Vol. 31, No. 3, 2008, pp. 751 – 764.

[20]Johnson, E. N., Calise, A. J., and Turbe, M. A., "Fault Tolerance through Direct Adaptive Control using Neural Networks," *Proc. AIAA Guidance, Navigation, and Control Conference and Exhibit*, AIAA, Reston, VA, USA, 2006.

[21]Suresh, S., Omkar, S. N., and Mani, V., "Direct Adaptive Neural Flight Controller for F-8 Fighter Aircraft," *Journal of Guidance, Control, and Dynamics*, Vol. 29, No. 2, 2006, pp. 454 – 464.

[22]Alwi, H., Edwards, C., Stroosma, O., and Mulder, J. A., "Fault Tolerant Sliding Mode Control Design with Piloted Simulator Evaluation," *Journal of Guidance, Control, and Dynamics*, Vol. 31, No. 5, 2008, pp. 1186 – 1201.

[23]Shtessel, Y. B. and Buffington, J., "Multiple Time Scale Flight Control Using Reconfigurable Sliding Modes," *AIAA Journal on Guidance, Control and Dynamics*, Vol. 22, No. 6, 1999, pp. 873–883.

[24]van Oort, E. R., Sonneveldt, L., Chu, Q. P., and Mulder, J. A., "A Comparison of Adaptive Nonlinear Control Designs for an Over-Actuated Fighter Aircraft Model," *AIAA Guidance, Navigation and Control Conference and Exhibit, Honolulu, Hawaii*, No. AIAA-2008-6786, 2008.

[25]Oliveira, J., Chu, Q. P., Mulder, J. A., Balini, H. M. N. K., and Vos, W. M., "Output Error Method and Two Step Method for Aerodynamic Model Identification," *AIAA Guidance, Navigation and Control Conference and Exhibit*, Aug. 2005.

[26]Khalil, H. K., *Nonlinear Systems*, Vol. third edition, Prentice Hall, 2002.

[27]Åström, K. J. and Wittenmark, B., *Adaptive Control*, Addison Wesley Longman, 1995, pp. 22, 91, 360.

[28]Farrell, J. A. and Polycarpou, M. M., *Adaptive Approximation Based Control, Unifying Neural, Fuzzy and Traditional Adaptive Approximation Approaches*, John Wiley & Sons, Inc., 2006.

[29]Polycarpou, M. M. and Ioannou, P. A., "A Robust Adaptive Nonlinear Control Design," *Automatica*, Vol. 32, No. 3, 1996, pp. 423 – 427.

[30]Freeman, R. A., Krstić, M., and Kokotović, P. V., "Robustness of Adaptive Nonlinear Control to Bounded Uncertainties," *Automatica*, Vol. 34, 1998, pp. 1227–1230.

[31]Krstić, M., Kanellakopoulos, I., and Kokotović, P. V., *Nonlinear and Adaptive Control Design*, Adaptive and Learning Systems for Signal Processing, John Wiley & Sons, Inc., 1995, pp. 186–187, 236.

[32]van Oort, E. R., Sonneveldt, L., Chu, Q. P., and Mulder, J. A., "Modular Adaptive Input-to-State Stable Backstepping of a Nonlinear Missile Model," *AIAA Guidance, Navigation and Control Conference and Exhibit, Hilton Head, South Carolina, Aug. 20-23*, 2007.

[33]Dehaene, J., Moonen, M., and Vandewalle, J., "Continuous-Time Recursive Least-Squares Estimation, Adaptive Neural Networks and Systolic Arrays," *IEEE Transactions on Circuits and Systems I: Fundamental Theory and Applications*, Vol. 42 (2), 1995, pp. 116 – 119.

[34]Stepanyan, V. and Hovakimyan, N., "Adaptive Disturbance Rejection Controller for Visual Tracking of a Maneuvering Target," *Journal of Guidance, Control, and Dynamics*, Vol. 30, No. 4, 2007, pp. 1090 – 1106.

[35]Cao, C. and Hovakimyan, N., "Vision-based aerial tracking using intelligent excitation," *American Control Conference, 2005. Proceedins of the*, Vol. 7, June 2005, pp. 5091 – 5096.

[36]Cao, C., Hovakimyan, N., and Wang, J., "Intelligent Excitation for Adaptive Control With Unknown Parameters in Reference Input," *Automatic Control, IEEE Transactions on*, Vol. 52, No. 8, Aug. 2007, pp. 1525–1532.

[37]de Boor, C., *A Practical Guide to Splines*, Springer-Verlag, 1978, pp. 87, 109.

[38]Nguyen, L. T., Ogburn, M. E., Gilbert, W. P., Kibler, K. S., Brown, P. W., and Deal, P. L., "NASA Technical Paper 1538 – Simulator Study of Stall/Post-Stall Characteristics of a Fighter Plane with relaxed Longitudinal Static Stability," Tech. Rep. 1538, NASA, Dec 1979.

[39]Duke, E. L., Antoniewicz, R. F., and Krambeer, K. D., "Derivation and Definition of a Linear Aircraft Model," Tech. Rep. RP-1207, NASA Ames Research Center Dryden Flight Research Facility, 1988.

[40]Sonneveldt, L., van Oort, E. R., Chu, Q. P., and Mulder, J. A., "Nonlinear Adaptive Trajectory Control Applied to an F-16 Model," *Journal of Guidance, Control, and Dynamics*, Vol. 32 (1), No. 0731-5090, 2009, pp. 25 – 39.

Downloaded by TECHNISCHE UNIVERSITEIT DELFT on December 30, 2013 | http://arc.aiaa.org | DOI: 10.2514/6.2010-7857